




3D Printing Materials for Physical Breast Phantoms: Monte Carlo Assessment and Experimental Validation

R. M. Tucciariello¹, P. Barca¹, D. Caramella⁴, R. Lamastra¹, A. Retico³, A. Traino²
and M. E. Fantacci^{1,3}

¹Department of Physics, University of Pisa, Pisa, Italy

²Unit of Medical Physics, Pisa University Hospital "Azienda Ospedaliero-Universitaria Pisana", Pisa, Italy

³INFN, Pisa Section, Pisa, Italy

⁴Department of Radiology, Pisa University Hospital "Azienda Ospedaliero-Universitaria Pisana", Pisa, Italy

Keywords: 3D-printing Materials, Breast Phantoms, Digital Mammography, Monte Carlo Simulations, Dosimetry, GEANT4, Radiochromic Films, XR-QA2, RADIOMA.


Abstract: The aim of this work is to characterize 3D-printing materials to be used for breast physical phantoms in mammography and digital breast tomosynthesis QA procedures or research. Our approach involves both Monte Carlo (MC) calculations and experimental measurements. Using a GEANT4-based application, MC simulations are involved in order to compare transmission properties of the digital "standard breast", which is composed by the external skin layer and the breast tissue inside, with those of typical printable materials. Substitute materials for skin layer and breast tissue have been identified and a 3D-printed physical breast phantom has been derived. Finally, a comparison between MC results and experimental measurements has been performed with the Hologic Selenia® Dimensions® mammography unit using XR-QA2 radiochromic films.


1 INTRODUCTION


In the last decades breast cancer screening programs have been introduced by public health services of many countries, highlighting an increasing involvement on early detection of breast masses. Indeed, breast cancer is the leading cause of cancer deaths in female subjects and tumour detection in an early stage ensures greater possibilities of treatment cures. Early detection and accurate diagnosis are carried out, in the last decades, with Digital Mammography (DM) and, in the last few years, with Digital Breast Tomosynthesis (DBT), a new pseudo-3D imaging modality (Sechopoulos 2013a, 2013b). X-ray mammography and breast tomosynthesis provide radiographic images of the compressed breast. In the first case two images for each breast are acquired (cranio-caudal and medio-lateral-oblique views), while in DBT the X-ray tube moves in an arc over the compressed breast and multiple projections

are acquired and then reconstructed by a computer, forming pseudo-three-dimensional images. The purpose of screening programs is to reduce breast cancer mortality by ensuring high quality services and optimized X-ray mammography units. This can be reached first of all with quality assurance (QA) protocols, which guarantee optimized equipment, and with training and research activities. Since both investigations use ionizing radiation, dosimetry assessment is mandatory.

Breast physical phantoms, which are test objects, represent fundamental tools used to perform quality assurance (QA) procedures and allow the calculation of useful parameters for imaging and radiation dosimetry. QA procedures and research are usually performed using polymethyl-metacrilate phantoms (PMMA), or other tissues simulating breast composition, which generally include objects representing mammographic lesions (tumour masses, fibers, microcalcifications), resolution patterns and

^a <https://orcid.org/0000-0001-9600-4177>

^b <https://orcid.org/0000-0003-3521-6293>

^c <https://orcid.org/0000-0003-2130-4372>

step wedges for assessing spatial resolution and contrast for the image quality assessment (Barca et al. 2019a; Barca et al. 2019b). The most used commercially physical phantoms for QA procedures are TORMAM (www.leadstestobjects.com) CDMAM (www.artinis.com), ACR (www.cirsinc.com). It is commonly assumed that a uniform PMMA block 45 mm thick is equivalent in absorption to a standard breast, which is a 5 cm thick compressed breast. It consists in a 40 mm thick central region comprising a certain mixture by weight of adipose tissue and glandular tissue (dependent on compressed breast thickness and age) surrounded by a 5 mm thick superficial layer of adipose tissue, simulating skin absorption (Perry et al. 2008).

Since breast glandularity¹ can vary from 0 to 100% and it strongly affects MGD, there is the need to consider this variable in physical phantoms, as well as in the MC simulations. Nevertheless, skin layer, not included in commercial phantoms, influences MGD and attenuation properties (Massera and Tomal 2018, Tucciariello et al. 2019).

The spread of the 3D-printing technology in the last years and the relatively inexpensive materials have led research groups to include printing materials in the context of medical physics and radiotherapy, for research, QA procedures and patient treatments (Ferreira et al. 2010; Madamesila et al. 2016). Nevertheless, 3D-printing is challenging due to variability of materials and printing methods, and an accurate characterization of printing materials is needed. Ivanov and colleagues (2018) explored 3D-printing materials exposing step-wedge phantoms with monochromatic beams at ESRF in Grenoble, in order to characterize attenuation coefficients.

The purpose of this study is to explore different 3D-printing materials which could be employed in the creation of new physical phantoms for DM and DBT which better represent both breast anatomy and X-ray attenuation properties. We propose the method used by our research group to define X-ray transmission properties of different materials using a DM X-ray source, widespread in clinics, and we introduce an experimental 3D-printed physical phantom. We made use of Monte Carlo (MC) simulations² and validated our method with experimental measurements using GAFchromic™ films.

¹ The term *glandularity* means the percentage of glandular tissue respect to the adipose tissue.

² The Monte Carlo method refers to a set of computational methods based on the use of artificially generated random numbers for solving phenomenon under investigation. In this case, photons

2 MATERIALS AND METHODS

Best practice in dosimetry purposes is to consider glandular tissue (a complex system of branched ducts that develop from the inside of the breast to the nipple) as the radiosensitive tissue in the breast. Thus, Mean Glandular Dose (MGD) is the parameter used to assess dose delivered to the glandular tissue. Since MGD is not a physical quantity, radiation dosimetry is performed using MC simulations thanks to the ability to estimate quantities that are challenging to measure empirically. This kind of approach makes use of certain geometry assumptions that depend on breast characteristics and allows to digitally reproduce a breast phantom model.

We investigated 3D-printing materials for physical breast phantoms, using the geometry assumptions followed by research groups whose works have been milestones for international dosimetry protocols (Boone 1999; Dance 1990; Dance, Young, and Van Engen 2011). Our approach involves both MC simulations as well as experimental measurements to validate our method.

2.1 Monte Carlo Model

Using the GEANT4 toolkit³, which is a C++ object-oriented toolkit for the simulation of particle through matter, we developed a MC code (Tucciariello et al. 2019) that reproduces mammographic and tomosynthesis investigations, with the same geometry assumptions (Figure 1) used for validation purposes (AAPM Task Group 2015). According to the prescriptions provided by the report of AAPM, the *Option4* PhysicsList was used in GEANT4, for the constructors and instances, designed for high accuracy in low-energy physics processes.

In MC models, breast digital phantom is modelled as a semi-cylinder with an outer layer of skin made by adipose tissue while the inner part is a homogeneous mixture of adipose and glandular tissues. Hammerstein et al. (1979) derived weight fraction of elements and total tissue density of both tissues (Table 1). Glandularities ranging from 0 to 100% are composed by mixing properly glandular and adipose tissues.

Polychromatic X-ray source has been implemented referring to the Hologic Selenia® Dimensions® mammography unit, with which

emitted by the X-ray source and interacting with the breast tissue are traced and all the interactions and dose deposits are registered.

³ <https://geant4.web.cern.ch/>

experimental measurements have been executed. An algorithm for tungsten anode spectral model has been involved, dubbed TASMIP_M (Boone, Fewell, and Jennings 1997), based on experimental measurements of mammography-energy X-ray spectra.

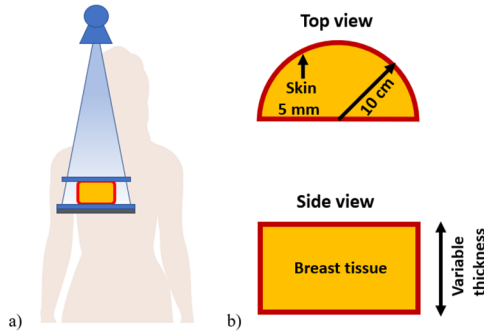


Figure 1: Schematic drawing of the (a) acquisition geometry for the cranio-caudal view in DM, and (b) breast phantom geometry adopted.

Table 1: Elemental composition and density of the two main constituents of the breast tissue.

Tissue	H	C	N	O	P	density (g/cm ³)
glandular	0.102	0.184	0.032	0.677	0.005	1.04
adipose	0.112	0.619	0.017	0.251	0.001	0.93

Since X-ray imaging is a transmission-based technique, X-ray transmission properties have been investigated involving *Air Kerma* (K) estimates. K can be easily defined in both experimental measurements, using e.g. an ionization chamber or radiochromic films, and in MC simulations. Air Kerma is the reference physical quantity for MGD evaluation purpose. Indeed, glandular dose estimates start from incident air kerma and then multiplying it for dedicated conversion factor from K to MGD, with the surface S for air kerma scoring placed under the compression paddle and on the upper surface of the breast. This formalism has been well defined in literature (Sarno et al. 2019) and is not the intend of this work.

For air kerma scoring, in our code we use the formalism provided by Sarno and colleagues (Sarno, Mettivier, and Russo 2017) using

$$K_{\text{air}} = \sum_i \frac{E_i \times \left(\frac{\mu_{\text{en}}}{\rho} (E_i) \right)_{\text{air}}}{S \cos(\vartheta_i)} \quad (1)$$

where E_i is the energy of the i th incident photon passes through the scoring surface S , $\left(\frac{\mu_{\text{en}}}{\rho} \right)_{\text{air}}$ is the air mass energy absorption coefficient at the

energy E_i (Hubbell and Seltzer 1995) and ϑ_i is the angle between the photon direction and the direction perpendicular to S .

In MC code, in order to define transmission properties of different materials, we simply place the air kerma scoring surface S inside a reference phantom 5 cm thick under the skin layer, or under the whole phantom, respectively to evaluate the influence of a certain material, e.g. skin layer or breast tissue. Data will be provided in terms of mGy per event, for both monoenergetic and polychromatic investigations.

In order to compare MC simulations results with experimental ones, we need to normalize both for a reference measurement that is the air kerma incident on the top of the phantom. The ratios in eq. (2) will be compared

$$\frac{K_{\text{air},m}^{\text{MC}}(d)}{K_{\text{air},inc}^{\text{MC}}} \cong \frac{K_{\text{air},m}^{\text{film}}(d)}{K_{\text{air},inc}^{\text{film}}} \quad (2)$$

which provides the transmission factors using MC simulations and GAFchromic films, where $K_{\text{air},m}(d)$ is the air kerma at a given depth d in the medium m , and $K_{\text{air},inc}$ is the incident air kerma on the upper side. In the paragraph 2.3 the formalism for obtaining $K_{\text{air}}^{\text{film}}$ will be presented.

Since MC results uncertainties are evaluated following Sempau et al. (2001), air kerma estimations are performed for monochromatic beams with 10^7 incident photons, while for polychromatic beams 10^8 primary photons are involved. These numbers let to obtain uncertainty on air kerma respectively tree and four orders of magnitude less. Uncertainties have not been introduced in all figures because they would not be visible.

2.2 3D-printing Materials

Breast tissue substitutes have been searched from few commercial low-cost 3D-printing materials. PLA, PET-G, ABS, PCABS, CARBON PA, GLASS PA, ASA have been investigated.

Since MC code needs for each material both elemental composition and density, using a A2v4 3D-printer⁴ we printed test objects for each one in order to define the printing precision and density⁵.

We used two simple parallelepiped solids of $10 \times 5 \times 80$ mm³ and $40 \times 40 \times 5$ mm³, and for each of them three copies were printed. Solids dimensions and weights were then measured and densities

⁴ www.3ntr.net

⁵ Is commonly known that after 3D-printing phase material density can change due to the extrusion printing procedure.

estimated. Due to the low printing reliability, CARBON PA and GLASS PA were rejected, while ASA material, despite the good printing quality, was avoided since it is a copolymer and its chemical formula can be different depending on the modality the three monomers repeat on the structure (Liu et al. 2011). A separate evaluation has been achieved for PCABS; because of not negligible variations in the test objects, we used a bigger test object to assess material density.

Elemental compositions of PLA, ABS, and PET-G have been taken from Alssabbagh et al. (2017), while for PCABS, polycarbonate composition is available on GEANT4 database (Table 2)⁶. Composition and density obtained were involved in MC simulations for evaluating transmission properties.

In the subsequent chapter the results that led to choose materials for the final physical phantom will be presented.

Table 2: Percentage elemental compositions of 3D-printing materials evaluated in our work.

Tissue	H	C	N	O	S	K
PLA	0.053	0.519	-	0.426	0.001	0.001
ABS	0.075	0.855	0.053	0.016	0.001	-
PET-G	0.075	0.652	-	0.271	0.002	-
Poly-carbonate	0.055	0.756	0	0.189	0	-
PCABS	80 % polycarbonate, 20% ABS					

2.3 Experimental Verification

Experimental verification of transmission properties for the 3D-printed materials was executed using GAFchromic™ XR-QA2 films. Radiochromic films are well suited for radiographic QA tests and research in dosimetry, thanks to the self-developing of the response after the irradiation process. XR-QA2 are designed for energies ranging in radiology, with anode tube potential ranging from 20 to 200 kVp.

XR-QA2 films are sensitive in the dose range 1-200 mGy and an increasing change in optical reflectance occurs with increasing doses.

2.3.1 Film Calibration and Digitization

Response of radiochromic films must be assessed with an accurate calibration in order to obtain a calibration curve, expressed in terms of air kerma versus reflectance change ΔR . Since Di Lillo et al.

(2016) showed energy dependant dose-response curves for XR-QA2 using synchrotron radiation, we proceeded to realize three calibration curves for 25, 30 and 35 kVp with the Hologic Selenia Dimensions in mammography modality. For each calibration curve 12 points were used, each of them is from the average value of 3 different radiochromic samples.

Since X-ray mammography units permits low-doses irradiations, in order to observe XR-QA2 dose range, a Radcal 20X6-60E ionisation chamber coupled with the 2026C dosimeter was used to choose correct mAs tube loading values and air kerma exposures, chosen in an optimal range from about 1 mGy to a maximum value depending on the kilovoltage applied.

The formalism defined by Tomic et al. (2010) and Di Lillo et al. (2016) was used and discussed above. From original XR-QA2 10×12" sheets, samples of 3×3 cm² have been cut to be used for calibrations and measurements. For calibration, 5 samples were used as "control films" to quantify background radiation and 36 samples for each calibration curve.

Using a flatbed scanner (Epson Expression 10000XL), samples were scanned before and after⁷ the exposition, in 48-bit RGB mode, at 150 dpi, in the same position of the scanner surface and saved as TIFF image file format. Multiple scans for each sample were executed. Raw images have been analysed with the open software *ImageJ*⁸. Formalism provides the film response in terms of reflectance change $\Delta R \pm \sigma_{\Delta R}$ using the 16-bit red channel in a ROI of 1×1 cm² in the center of each sample (Figure 2).

$$\Delta R = \frac{1}{2^{16}} (PV_{before} - PV_{after}) \quad (3)$$

$$\sigma_{\Delta R} = \frac{1}{2^{16}} \sqrt{(\sigma_{PV_{before}})^2 + (\sigma_{PV_{after}})^2 + (\sigma_{scanner})^2} \quad (4)$$

where PV_{before} and PV_{after} are the mean pixel value of samples respectively before and after the X-ray exposition, and $\sigma_{PV_{before}}$ and $\sigma_{PV_{after}}$ the standard deviations.

Statistical uncertainty due to scanner response in multiple scans is included in $\sigma_{scanner}$. The final value is considered

$$net\Delta R = \Delta R - \Delta R_{control} \quad (5)$$

with the relative uncertainty

⁶ PCABS is composed by polycarbonate and ABS. The percentage of ABS can be different depending on manufactures.

⁷ Scans for irradiated samples have been executed 24h after the exposition.

⁸ <https://imagej.nih.gov/ij/>

$$\sigma_{\text{net}\Delta R} = \frac{1}{2^{16}} \sqrt{(\sigma_{\Delta R})^2 + (\sigma_{\Delta R_{\text{control}}})^2} \quad (6)$$

Calibration data points have been fitted using the commercial analysis software Origin 9⁹ and using the exponential function $y = a \cdot x \cdot e^{bx}$.

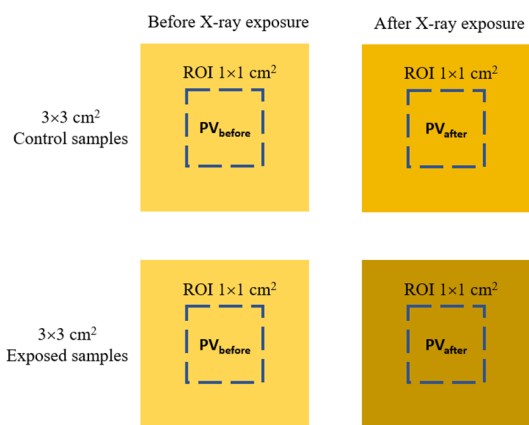


Figure 2: Scheme of radiochromic samples before and after the exposure, and ROI used for the pixel values estimation.

3 RESULTS

3.1 Density Assessment

Our first purpose was to evaluate the change in density for different materials from the coil nominal density value to the post-printed value. Test objects reported variation between -9% and -14% and reported in Table 3. PCABS final density has been evaluated with a bigger test object which presented a different value in density respect to the smaller objects, suggesting a “form factor” influencing printed objects density depending on dimensions.

Table 3: Change in density for the materials under investigation. The uncertainty on the estimated density is 0.01 g/cm³.

[g/cm ³]	PLA	ABS	PET-G	PCABS	ASA
Nominal density	1.24	1.05	1.27	1.13	1.07
Estimated density	1.12	0.92	1.09	0.99	0.97
variation	-10%	-12%	-14%	-12%	-9%

3.2 MC Assessment

Data provided in tables 1-3 were used in MC simulations in order to compare transmission

properties of adipose skin layer and breast tissue with those of 3D-printing material.

3.2.1 Skin Layer

Using the simulation setup shown in Figure 1, a reference phantom 5 cm thick, 50% glandular, and a skin thickness of 5 mm made by adipose tissue has been adopted. We placed a scoring surface below the skin and evaluated the air kerma transmission curve through the skin due to monoenergetic X-ray beams, from 8 to 40 keV at 1 keV steps. Using this approach, we replaced adipose tissue composing the skin layer with 3D-printing materials with density correction. MC simulations were performed with 10⁷ incident photons for each energy beam. Results are shown in Figure 3. At lower photon energies, the skin “shields” the breast tissue and air kerma values are low; with increasing photon energies X-ray beam penetrates the skin layer up to a maximum value after which K decreases due to the decreasing energy absorption coefficient. Simulations suggest a better behaviour by PCABS as skin layer respect to the other material, for both low- and high-energies.

Since DM and DBT use polychromatic X-ray source, we investigated polyenergetic X-ray beams @ 27, 31 and 35 kV, in W/Rh anode/filter combination. In Figure 4 is shown air kerma transmission through the skin layer using polychromatic beams. MC simulations were performed using 10⁸ incident photons. Air kerma values percentage variations, respect to the adipose skin layer, suggest also in this case that PCABS is a well substitute as skin layer.

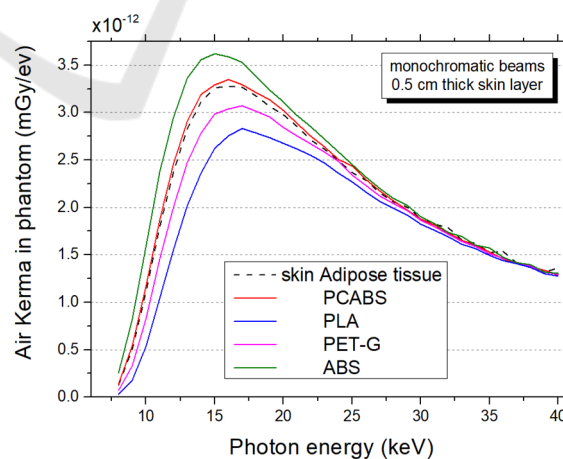


Figure 3: Air kerma transmission through the skin layer due to monoenergetic beams.

⁹ www.originlab.com

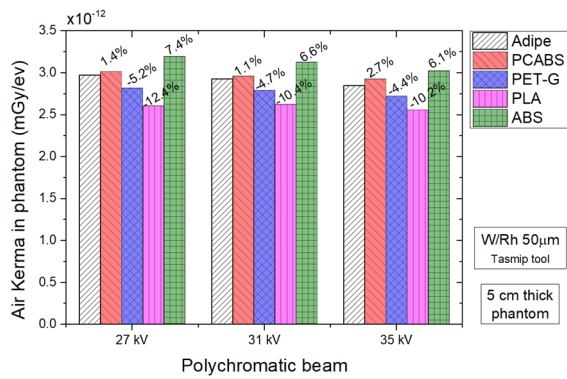


Figure 4: Air Kerma transmission through the skin layer due to polychromatic beams. Percentage values in figure refer to the variation respect to the adipose tissue.

3.2.2 Breast Tissue

Using the same approach of the previous paragraph, we investigated 3D-printing materials for the inner part of the breast phantom assuming PCABS as the preferred skin layer material. We used, as usual, the reference breast phantom cited previously. Figure 5 shows that both PLA and PETG can be used for the inner part of the breast phantom, coupled with 5 mm thick PCABS skin layer.

Since in literature there are studies involving the amount of glandular fraction of women breast, we noted a publication of Yaffe et al. (2009) whose work found that, out of 2831 women, 95% were below the 45% glandularity. We show 0% glandularity transmission curve in order to define the “range” of transmission which 3D-materials have to follow.

Polychromatic beams have been investigated and results are reported in Figure 6.

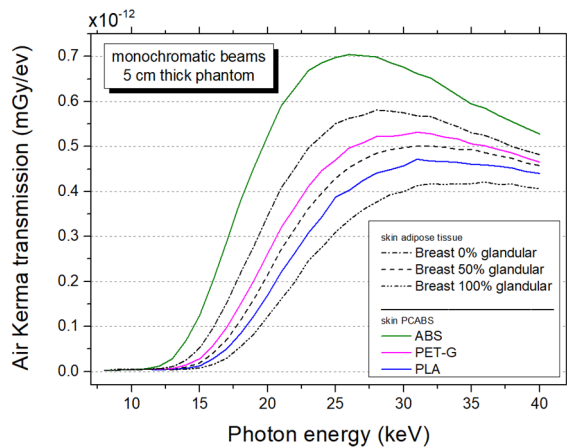


Figure 5: Air kerma transmission through the whole phantom for monochromatic beams.

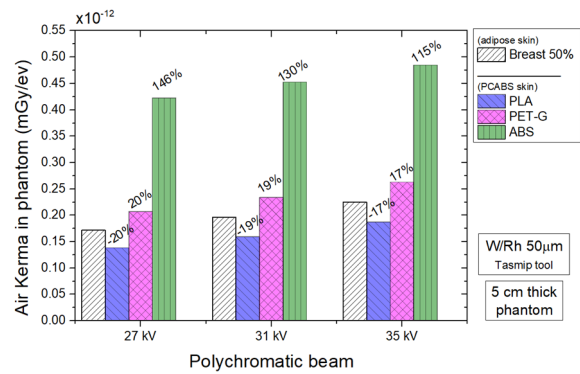


Figure 6: Air kerma transmission through the whole phantom for polychromatic beams. Percentage values in figure refer to the variation respect to the breast 50% glandular.

3.2.3 Film Calibration Curves

Results from calibration procedure of GAFchromic films XR-QA2 free-in-air are shown in Figure 7. Energy dependant response curve is slightly marked, where the beam mean energy is for 25, 30 and 35 kV respectively 18.4, 19.1 and 20.0 keV. Points in the graph are scattered from about 1 to 2 mGy and follow the fit curve for doses higher than 2 mGy.

Even if digital mammography is a low-exposure procedure, it is worth noting that high milliamperages have been used in order to have a major statistic in the calibration curves, which otherwise would be affected too much by the low exposure fluctuations.

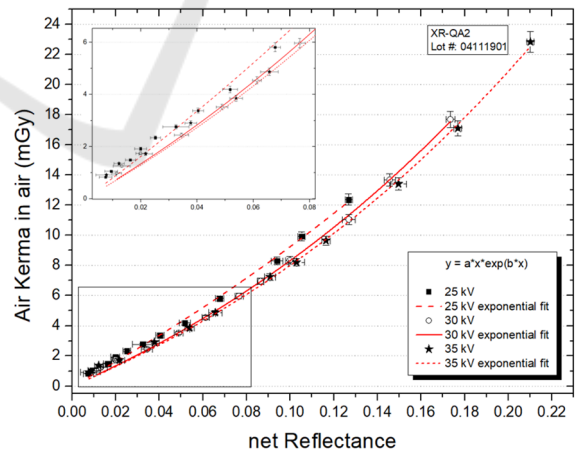


Figure 7: Calibration curves @ 25, 30 and 35 kV. In figure is shown a magnification for low-doses exposures.

3.3 3D-printed Phantom Dosimetry Assessment

Results from the previous investigations led to create a breast phantom with an outer layer made by PCABS material and an inner part of PLA material.

Despite of PETG curve is between those of glandularities 0% and 50% (Figure 5), we decide to characterize experimentally PLA because during the 3D-printing phase, density can be further changed with the *infill* option, that is the percentage of air filling (Madamesila et al. 2016). This can cause a major X-ray transmission depending on the infill percentage. Using this approach, a greater number of glandularities can be explored, from more than 50% to 0%, incrementing the infill option. Infill option has not been investigated yet, and our purpose is first of all to evaluate experimentally our method and PCABS+PLA physical phantom.

Using the open software FreeCAD¹⁰, we developed a modular 3D phantom made by few slices in order to compose different breast phantom thicknesses. Each component of the phantom is exported in STL file format used by the 3D printer. Phantom is composed by external layers (in grey, Figure 8) printed in PCABS, and PLA inner components (in orange). As reported in Figure 1, radius semi-cylinder is 10 cm, while thickness is variable depending on how many slices are used. Slices let to perform dosimetry with radiochromic films by inserting below each layer a 3×3 cm² GAFchromic sample (Figure 9).

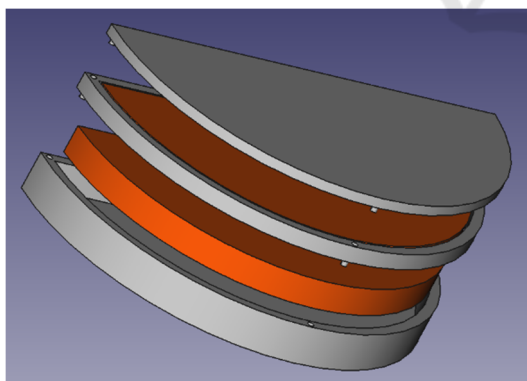


Figure 8: 3D project of the modular phantom created.

In order to demonstrate the agreement with transmission properties of the physical phantom with the expected values from MC simulations, a comparison has been performed. Following equation (2), experimental measurements have been performed

¹⁰ <https://www.freecadweb.org/>

@ 35 kV by inserting radiochromic film samples under each slice of the phantom for obtaining $K_{air,m}^{film}(d)$ at a given depth d , normalized by $K_{air,inc}^{film}$ obtained placing samples between the phantom surface and the compression paddle.

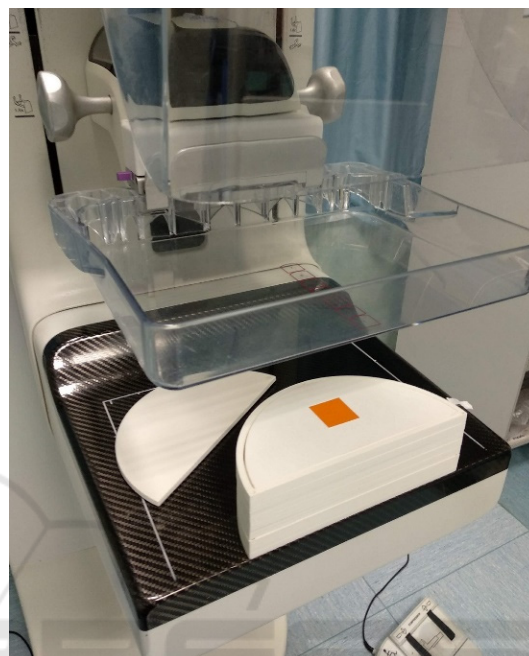


Figure 9: Example of positioning of radiochromic sample inside the phantom. The photograph refers to the $K_{air,m}^{film}(0.5)$ value obtained under the upper PCABS skin layer which has been temporary removed for placing the sample.

MC simulations refer to air kerma estimates at the same depth in the phantom. Results in Table 4 show a good agreement in transmission properties of the skin layer (depth 0.5 mm) and the firsts two PLA layers (depth 1.3 and 2.1 mm); in the last layers the discrepancy is greater, because of the low doses reached. Indeed, air kerma estimates derived from the fitting curve show values from about 2 mGy to 0.8 mGy, not considered reliable. This is a limitation due to characterizing low dose in mammography, especially in the phantom lower layers, with subsequent low dose exposures in radiochromic films. This does not allow to complete the *percentage depth dose* curve.

Table 4: Comparison between experimental data with MC simulations. Variations in the last column have been obtained using equation 2. The first row (in grey) represents the transmission due to the 5 mm thick PCABS layer, while the other (orange) rows the transmission due to the 8 mm thick PLA layers composing the phantom inner part.

Depth d (mm)	$netAR$	$K_{air}^{film}(d)$ (mGy)	$K_{air}^{MC}(d)$ (mGy/ev)	variation
<i>Inc</i>	0.1461	13.22	3.78 E-12	-
0.5	0.1205	10.19	2.98 E-12	-2.5%
1.3	0.0806	6.14	1.77 E-12	-1.1%
2.1	0.0530	3.75	1.09 E-12	-1.7%
2.9	0.0329	2.15	6.73 E-12	-9.7%
3.7	0.0207	1.35	4.23 E-12	-9.9%
4.5	0.0132	0.84	2.74 E-12	-14.4%

4 DISCUSSION

We presented the method used by our research group to characterize 3D-printing materials to be used for the creation of breast physical phantoms, having the same transmission properties of the digital breast phantoms used in MC breast dosimetry, whose have dedicated elemental compositions for adipose and glandular tissues. The approach of involving physical phantoms with dedicated materials for the skin and the for the breast tissue could be useful in research or QA procedures for DM and DBT investigations, where, until now, polymethyl-metacrilate homogeneous phantoms are used. We involved MC simulations to investigate transmission properties of some 3D-printing materials, whose densities have been corrected in the MC code, since the final density of the printed object can vary during the printing phase. Based on the MC results, performed over monoenergetic and polyenergetic beams, a physical breast phantom has been created. Results deriving from densities estimation and MC simulations led to consider PCABS material as a well substitute for the 5 mm thick skin layer and PLA material as substitute for the inner breast tissue.

In order to validate our test phantom, experimental measurements with GAFchromic XR-QA2 films were performed, which results confirmed an agreement with transmission estimations in MC results for both PCABS layer and for the inner PLA material, supporting our method, which uses relatively low-cost equipment and procedures.

Since it is known that mostly of women breast glandularities ranging from 0% to about 50%, we decided to adopt PLA material, to support our next step, which will be to characterize the *infill* option that allows to decrease voluntarily the material density during the printing phase. With this approach

various breast glandularities from 0 to about 50% can be reached in synthetic phantoms, leading to perform the image quality assessment for different synthetic breast anatomies.

ACKNOWLEDGEMENTS

The presented work is part of the RADIOMA project which is partially funded by "Fondazione Pisa", Technological and Scientific Research Sector, Via Pietro Toselli 29, Pisa (Italy). The authors would like to thank Fondazione Pisa for giving the opportunity to start this study.

REFERENCES

- Alssabbagh, M., Tajuddin, A. A., Abdulmanap, M. and Zainon, R., 2017. *Evaluation of 3D Printing Materials for Fabrication of a Novel Multi-Functional 3D Thyroid Phantom for Medical Dosimetry and Image Quality*. Radiation Physics and Chemistry 135: 106–12. <http://dx.doi.org/10.1016/j.radphyschem.2017.02.009>.
- Barca, P. et al. 2019. *Image Quality Comparison between Digital and Synthetic 2D Mammograms: A Qualitative and Quantitative Phantom Study*. BIOIMAGING 2019 - 6th International Conference on Bioimaging, Proceedings; Part of 12th International Joint Conference on Biomedical Engineering Systems and Technologies, BIOSTEC 2019: 129–36.
- Barca, P., et al. 2019. *Comprehensive Assessment of Image Quality in Synthetic and Digital Mammography: A Quantitative Comparison*. Australasian Physical & Engineering Sciences in Medicine (Cd).
- Boone, J. M., 1999. *Glandular Breast Dose for Monoenergetic and High-Energy x-Ray Beams: Monte Carlo Assessment*. Radiology 213(1): 23–37.
- Boone, J. M., Fewell, T. R. and Jennings, R. J., 1997. *Molybdenum, Rhodium, and Tungsten Anode Spectral Models Using Interpolating Polynomials with Application to Mammography*. Medical Physics 24(12): 1863–74.
- Dance, D. R., 1990. *Monte-Carlo Calculation of Conversion Factors for the Estimation of Mean Glandular Breast Dose*. Physics in Medicine and Biology 35(9): 1211–19.
- Dance, D. R., Young, K. C. and Van Engen, R. E., 2011. *Estimation of Mean Glandular Dose for Breast Tomosynthesis: Factors for Use with the UK, European and IAEA Breast Dosimetry Protocols*. Physics in Medicine and Biology 56(2): 453–71.
- Ferreira, C. C. et al., 2010. *Evaluation of Tissue-Equivalent Materials to Be Used as Human Brain Tissue Substitute in Dosimetry for Diagnostic Radiology*. Nuclear Instruments and Methods in Physics Research, Section B: Beam Interactions with Materials and Atoms

- 268(16): 2515–21. <http://dx.doi.org/10.1016/j.nimb.2010.05.051>.
- Hammerstein, G. R. et al., 1979. *Absorbed Radiation Dose in Mammography*. Radiology 130(2): 485–91.
- Hubbell, J. H., and Seltzer, S. M., 1995. *Tables of X-Ray Mass Attenuation Coefficients and Mass Energy-Absorption Coefficients 1 KeV to 20 MeV for Elements Z=1 to 92 and 48 Additional Substances of Dosimetric Interest*. [Http://Physics.Nist.Gov/Xaamdi](http://Physics.Nist.Gov/Xaamdi) 5632. <http://www.nist.gov/pml/data/xraycoef/index.cfm>.
- Ivanov, D. et al., 2018. *Suitability of Low Density Materials for 3D Printing of Physical Breast Phantoms*. Physics in Medicine and Biology 63(17): aad315. <https://doi.org/10.1088/1361-6560/aad315>.
- Di Lillo, F. et al., 2016. *Energy Dependent Calibration of XR-QA2 Radiochromic Film with Monochromatic and Polychromatic x-Ray Beams*. Medical Physics 43(1): 583–88.
- Liu, S. et al., 2011. *Reactive Compatibilization of Poly (Butylene Terephthalate)/Acrylonitrile- Styrene-Acrylate Blends by Epoxy Resin: Morphology and Mechanical Properties*. Journal of Macromolecular Science, Part B: Physics 50(9): 1780–90.
- Madamesila, J., McGeachy P., J. Barajas, E. J. and Khan, R., 2016. *Characterizing 3D Printing in the Fabrication of Variable Density Phantoms for Quality Assurance of Radiotherapy*. Physica Medica 32(1): 242–47. <http://dx.doi.org/10.1016/j.ejmp.2015.09.013>.
- Massera, R. T. and Tomal, A., 2018. *Skin Models and Their Impact on Mean Glandular Dose in Mammography*. Physica Medica 51: 38-47.
- Perry, N. et al., 2008. *European Guidelines for Quality Assurance in Breast Cancer Screening and Diagnosis. Fourth Edition - Summary Document*. Annals of Oncology 19(4): 614–22. http://europa.eu.int/comm/dgs/health_consumer/index_en.htm.
- Sarno, A. et al., 2019. *Monte Carlo Calculation of Monoenergetic and Polyenergetic DgN Coefficients for Mean Glandular Dose Estimates in Mammography Using a Homogeneous Breast Model*. Physics in medicine and biology 64(12): 125012.
- Sarno, A., Mettivier, G. and Russo, P., 2017. *Air Kerma Calculation in Monte Carlo Simulations for Deriving Normalized Glandular Dose Coefficients in Mammography*. Physics in Medicine and Biology.
- Sechopoulos, I., 2013a. *A Review of Breast Tomosynthesis. Part I. The Image Acquisition Process*. Medical Physics.
- . 2013b. *A Review of Breast Tomosynthesis. Part II. Image Reconstruction, Processing and Analysis, and Advanced Applications*. Medical Physics.
- Sempau, J. et al., 2001. *Monte Carlo Simulation of Electron Beams from an Accelerator Head Using PENELOPE*. Physics in Medicine and Biology 46(4): 1163–86.
- Task Group, Aapm. 2015. *Monte Carlo Reference Data Sets for Imaging Research*. Medical Physics 42. <http://dx.doi.org/10.1118/1.4928676>.
- Tomic, N., Devic, S., Deblois, F. and Seuntjens, J., 2010. *Reference Radiochromic Film Dosimetry in Kilovoltage Photon Beams during CBCT Image Acquisition*. Medical Physics 37(3): 1083–92.
- Tucciariello, R. M. et al., 2019. *Monte Carlo Methods for Assessment of the Mean Glandular Dose in Mammography: Simulations in Homogeneous Phantoms*. BIOINFORMATICS 2019 - 10th International Conference on Bioinformatics Models, Methods and Algorithms, Proceedings; Part of 12th International Joint Conference on Biomedical Engineering Systems and Technologies, BIOSTEC 2019: 242–49.
- Yaffe, M. J. et al., 2009. *The Myth of the 50-50 Breast*. Medical Physics 36(12): 5437–43.